Journal of Materials and Environmental Sciences
ISSN : 2028-2508
CODEN : JMESCN

J. Mater. Environ. Sci., 2018, Volume 9, Issue 1, Page 345-357

https://doi.org/10.26872/jmes.2018.9.1.38

http://www.jmaterenvironsci.com

Experimental and theoretical studies of 5-((4-phenyl-4,5-dihydro-1H-tetrazol-1-yl)methyl)quinolin-8-ol quinoline derivative as effective corrosion inhibitor for mild steel in 1.0 M HCl

H. About[1,2], M. El faydy[2], Z. Rouifi[1,2], F. Benhiba[1], H. Ramsis[3], M. Boudalia[4], H. Zarrok[1], H. Oudda[1], R. Touir[5,6], M. El M'Rabet[7], I. Warad[8], A. Guenbour[3], B. Lakhrissi[2]

[1] *Laboratory of Separation Processes, Faculty of Science, University IbnTofail, Kenitra, Morocco.*
[2] *Laboratory of Agro-Resources, Polymers and Process Engineering, Department of Chemistry, Faculty of Science, Ibn Tofail University, PO Box 133, 14000, Kenitra, Morocco*
[3] *Laboratoire de Spectroscopie, Département de Chimie, Faculté des sciences, Université Ibn Tofail, Kenitra, Morocco*
[4] *Laboratory of Electrochemistry, Corrosion and Environment, Faculty of science, Rabat, Morocco.*
[5] *Laboratoire d'Ingénierie des Matériaux et d'Environnement : Modélisation et Application, Faculté des Sciences, Université Ibn Tofail, BP 133, Kénitra 14 000, Morocco.*
[6] *Centre Régional des Métiers de l'Education et de la Formation (CRMEF), Avenue Allal Al Fassi, Madinat Al Irfane BP 6210 Rabat, Morocco.*
[7] *Département DSFA, Unité de chimie, Institut Agronomique et Vétérinaire Hassan II. Rabat, Morocco.*
[8] *Department of Chemistry, AN-Najah National University P.O. Box 7, Nablus, Palestine.*

Received 20 Mar 2017,
Revised 14 May 2017,
Accepted 19 May 2017

Keywords

- ✓ Synthesis;
- ✓ Corrosion inhibition;
- ✓ Quinoline derivatives;
- ✓ Mild steel;
- ✓ DFT.

Pr. H Oudda
ouddahassan@gmail.com
+212698192251

Abstract

A new organic inhibitor, namely 5-((4-phenyl-4,5-dihydro-1H-tetrazol-1-yl)methyl)quinolin-8-ol, denoted **PTQ8** was synthesized and characterized using ^{1}H and ^{13}C NMR spectroscopies. Thus, its corrosion inhibition on mild steel in 1.0 M HCl solution was investigated by weight loss and electrochemical measurements. The experimental results were supported by DFT calculations. The temperature effect on the corrosion behaviour of mild steel in 1.0 M HCl without and with **PTQ8** was studied in the temperature range 298–328 K. The results showed that the inhibition efficiency of **PTQ8** increases with concentration and decreases with temperatures. The associated activation energy has been determined and discussed. It is found that the adsorption of **PTQ8** on the mild steel surface obeys to the Langmuir's adsorption isotherm. It is found also that the theoretical calculations are in good agreement with the experiments results.

1. Introduction

The use of inhibitors to prevent corrosion of metals is an extremely important area. Many chemical substances are used to protect metals against degradation due to corrosion, in particular in acidic medium [**1**]. The most important fields of acid solutions application being the acid pickling, industrial cleaning and descaling. The use of acidic solutions in these industrial processes results a considerable metal corrosion. In order to reduce corrosive attack on metallic materials inhibitors are widely used [**2**]. The most effective and efficient inhibitors are organic compounds containing nitrogen, sulfur, oxygen atoms and multiple bonds which they act by adsorption mechanism [**3-14**].

According to the literature, many N-heterocyclic compounds such as pyrimidine derivatives [**15**], the tetrazole derivatives [**16**], triazole derivatives [**17**] were used for the corrosion inhibition of iron or steel in acidic media. The quinoline derivatives are one of the important constituents of pharmacologically active synthetic compounds [**18**], including biological activities [**19**]. Accordingly, the corrosion inhibition study and inhibition mechanism is necessary of new inhibitor containing 8-hydroxyquinoline in their structure.

In the present work, the 5-((4-phenyl-4,5-dihydro-1H-tetrazol-1-yl)methyl)quinolin-8-ol (**PTQ8**) newly synthesized and investigated as corrosion inhibitors of mild steel in 1.0 M HCl by weight loss, electrochemical measurements coupled with theoretical studies.

2. Materials and methods

2.1. Synthesis of PTQ8

❖ **General Information**

All chemicals products were purchased from Aldrich or Acros (France). The melting points were determined on an automatic electrothermal IA 9200 digital. ^{1}H and ^{13}C NMR spectra were recorded on a model Bruker Avance (300 MHz) for solutions in Me_2SO-d6. Chemical shifts are given as δ values with reference to tetramethylsilane (TMS) as internal standard. The progress of the reaction was followed by Thin-Layer Chromatography (TLC) using silica gel 60 F254 (E. Merck) plates with visualization by UV light (254 nm).

❖ **Chemical synthesis**

Synthesis of 5-((4-phenyl-4,5-dihydro-1H-tetrazol-1-yl)methyl)quinolin-8-ol (PTQ8)

At first, the 5-chloromethyl-8-quinolinol hydrochloride (1) was prepared according to method reported in literature (Scheme1) [**20**].

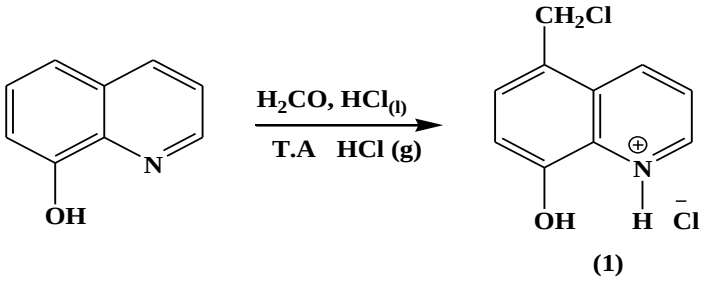

Scheme 1: 5-Chloromethyl-8-quinolinol hydrochloride (1)

5-Chloromethyl-8-quinolinol hydrochloride (**1**) was converted into 5-azidomethyl-8-quinolinol (**2**) according to the following reaction scheme 2.

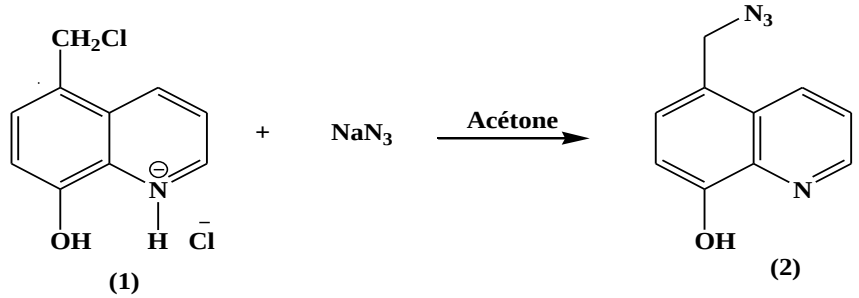

Scheme 2: 5-azidomethyl-8-quinolinol (2)

The synthesis of -((4-phenyl-4,5-dihydro-1H-tetrazol-1-yl)methyl)quinolin-8-ol (**PTQ8**) is described according to the following reaction scheme 3.

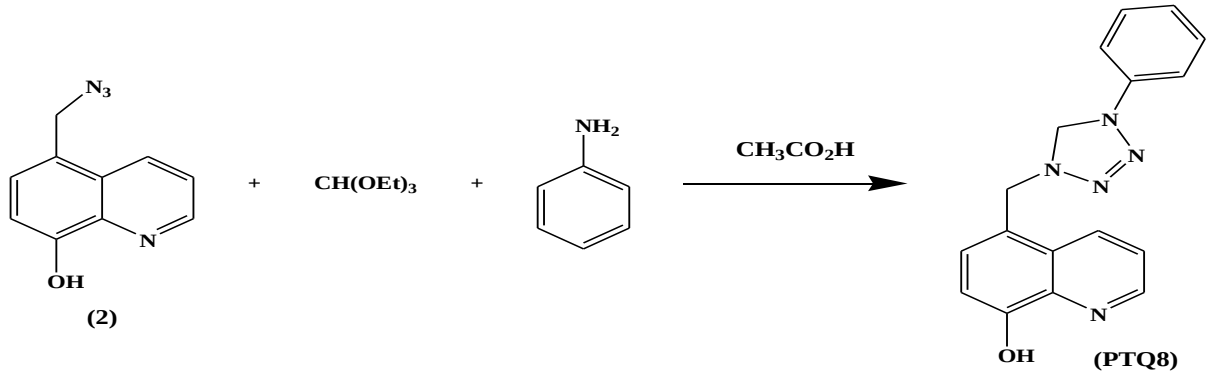

Scheme 3: 5-((4-phenyl-4, 5-dihydro-1H-tetrazol-1-yl) methyl) quinolin-8-ol (**PTQ8**)

Synthesis of 5-((4-phenyl-4, 5-dihydro-1H-tetrazol-1-yl) methyl) quinolin-8-ol (PTQ8)

Acetic acid was added with stirring to a suspension of aniline (5×10^{-3} mol), and 5-azidomethyl-8-quinolinol (1 g, 5×10^{-3} mol) in triethyl orthoformate (5×10^{-3} mol), and the mixture was refluxed for 12 hours. The progress of the reaction was monitored by TLC using hexane-acetone (4:6, v/v) as eluent. The mixture was neutralized by NaOH addition and then it was extracted with dichloromethane. The organic phase was recovered and dried over anhydrous $MgSO_4$ and then evaporated. The residue obtained was purified by silica gel column chromatography with n-hexane-acetone mixture (6:4, v/v) as the mobile phase, to give 5-((4-phenyl-4, 5-dihydro-1H-tetrazol-1-yl) methyl) quinolin-8-ol (**PTQ8**)

The structure of the new prepared product (**PTQ8**) was confirmed by ^{1}H NMR and ^{13}C NMR spectra.

^{1}H NMR (300 MHz, DMSO-d6), δppm = 9.06-9.07 (s, 1 H, quinoline (C-OH)), 7.30-8.64 (m, 11 H, quinoline and benzene), 3.78 (s, 2 H, quinoline-CH_2-N), 4.50 (s, 2 H, N-CH_2-N), 2.28 (s, H of trace H_2O present in DMSO-d6).

^{13}C NMR (300 MHz, DMSO-d6) δppm: 24.65(quinoline-CH_2-N), 111.32- 148.37 (Aromatic: quinoline and benzene), 152.74 (quinoline C=N), 168.92 (quinoline C-OH).

^{1}H NMR spectra (300 MHz, Me2SO-d6)

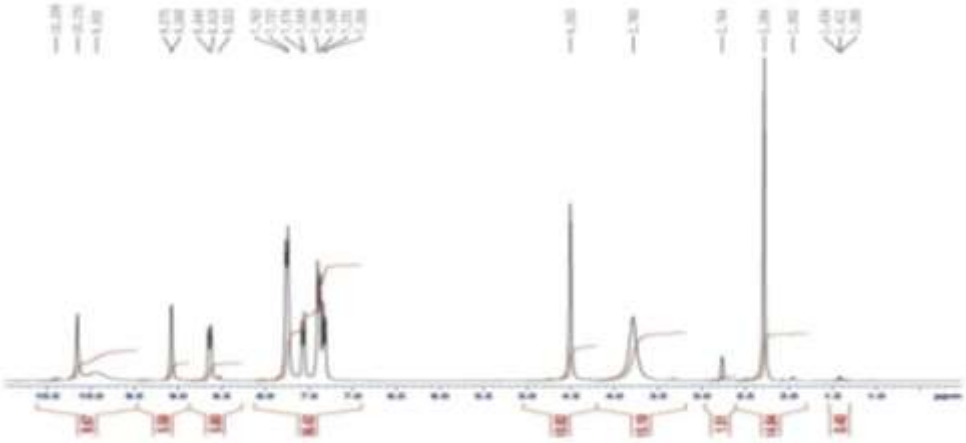

Figure 1: ^{1}H NMR spectrum of 5-((4-phenyl-4, 5-dihydro-1H-tetrazol-1-yl) methyl) quinolin-8-ol (**PTQ8**)

^{13}C NMR spectra (300 MHz, Me2SO-d6)

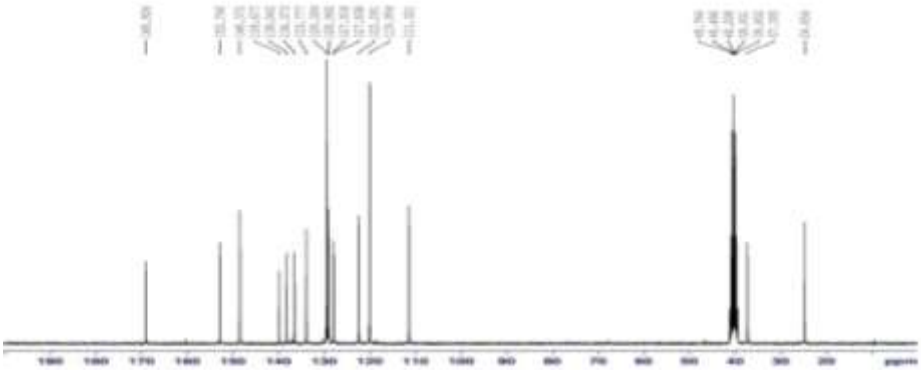

Figure 2: ^{13}C NMR spectrum of 5-((4-phenyl-4, 5-dihydro-1H-tetrazol-1-yl) methyl) quinolin-8-ol (**PTQ8**)

2.2. Gravimetric, Electrochemical measurements and Electrolytic solution

The mild steel specimen used in this study had a rectangular form (1.5 cm×1.5 cm×0.3 cm) with a chemical composition (in wt.%) of 0.09 % P; 0.38 % Si; 0.01 % Al; 0.05 % Mn; 0.21 % C; 0.05 % S and the remainder iron were used for gravimetric studies. The surface of the test electrode was mechanically abraded by different grades of emery papers with 220 up to 1200, rinsed with distilled water, cleaned with acetone and finally dried at hot temperature. Then, the loss in weight was determined by analytic balance after 6 h of immersion at 298 K. Three tests were performed in each case and the mean value of the weight loss was calculated.

For electrochemical studies, the experimental apparatus used is the potentiometer PGZ 100, controlled by a PC computer and the software Voltamaster 4.0. The potentiodynamic polarization curves and electrochemical impedance spectroscopy (EIS) were carried out in a standard three-electrode cell. The saturated calomel electrode (SCE) and the platinum electrode were used as reference and auxiliary electrode, respectively while

the mild steel specimen was used as working electrode with exposed surface area of 1 cm^2. The working electrode was immersed in test solution for 30 minutes to attain a steady state open circuit potential (*E*ocp). After the determination of *E*ocp, the electrochemical measurements were performed. The impedance diagrams are given in the Nyquist representation. The EIS measurements were performed with a frequency range of 10 mHz to 100 kHz and amplitude of 5 mV with 10 points per decade. The aggressive solutions of 1.0 M HCl were prepared by dilution of analytical grade 37 % HCl with distilled water. The concentration range of 5-((4-phenyl-4,5-dihydro-1H-tetrazol-1-yl)methyl)quinolin-8-ol **(PTQ8**) used was 10^{-6} M to 10^{-3}M.

2.3. Quantum chemical calculations

Quantum chemical calculations are used to correlate experimental data for inhibitors obtained from different techniques and their structural and electronic properties [**21**]. Quantum chemical calculations were performed by density functional theory (DFT) level with the non-local correlation functional B3LYP, combining Becke's three-parameter exchange functional with the correlation functional of Lee et al. at basis sets 6-31G(d,p) **[22, 23]**. DFT calculations were carried out using the Gaussian-03 program package. The following quantum chemical indices were considered: the energy of the highest occupied molecular orbital (E_{HOMO}), the energy of the lowest unoccupied molecular orbital (E_{LUMO}), energy band gap $\Delta E = E_{HOMO}-E_{LUMO}$, the electron affinity (A), the ionization potential (I) and the number of transferred electrons (ΔN).

3. Results and discussion

3.1. Weight loss measurements

The corrosion of mild steel in 1.0 M HCl medium containing various concentrations of **PTQ8** at 298 K was studied by weight loss measurements. The values of inhibition efficiency and corrosion rate (C_R) are presented in Table 1. In this case, the inhibition efficiency (η_w (%) is calculated by applying the following equation :

$$\eta_w = \frac{C_R - C_R^{inh}}{C_R} \times 100 \qquad (1)$$

where C_R and C^{inh}_R represent the corrosion rates in the absence and presence of **PTQ8**, respectively.

Table 1. Inhibition efficiencies of various concentrations of **PTQ8** for mild steel corrosion in 1.0 M HCl obtained by weight loss measurement at 298 K.

	Conc. (M)	C_R (mg cm^{-2} h^{-1})	η_w (%)	θ
Blank solution	00	0.429	-	-
PTQ8	10^{-6}	0.140	67.2	0.672
	10^{-5}	0.112	73.7	0.737
	10^{-4}	0.087	79.72	0.7972
	10^{-3}	0.068	84.1	0.841

The analysis of the data in Table 1 shows a net decrease of the corrosion rate of mild steel in 1.0 M HCl medium in the absence and presence of **PTQ8**. It is noted also that they the inhibition efficiency increases with **PTQ8** concentration. This may be interpreted by the presence of cyclic rings and heteroatoms which facilitate the adsorption process.

3.2. Potentiodynamic polarization curves

Figure 1 shows current–potential characteristics resulting from cathodic and anodic polarization curves of mild steel in 1.0 M HCl without and with different concentrations of **PTQ8**. It is noted that the addition of **PTQ8** has the effect of reducing both anodic and cathodic currents and small variations in the E_{corr} value, indicating that **PTQ8** is a mixed type inhibitor. Thus, the nature of polarization curves indicates that the inhibitor influence both the anodic and cathodic reactions resulting in delay of anodic dissolution of metal and cathodic hydrogen evolution reaction through blocking the active reaction sites on metal surface while in the activation energy barriers of anodic and cathodic reactions, no change occurs [**24,25**]. This means that the hydrogen evolution reaction on the mild steel surface follows a charge transfer mechanism.

However, the electrochemical parameters such as corrosion current density (i_{corr}), corrosion potential (E_{corr}) and cathodic Tafel slope (β_c) obtained by curve fitting using the equation:

$$i = i_a + i_c = i_{corr}\left\{\exp\left[b_a \times \left(E - E_{corr}\right)\right] - \exp\left[b_c \times \left(E - E_{corr}\right)\right]\right\} \qquad (2)$$

where i_{corr} is the corrosion current density (A cm^{-2}), b_a and b_c are the Tafel constants of anodic and cathodic reactions (V^{-1}), respectively.

These constants are linked to the Tafel slopes β (V/dec) in usual logarithmic scale given by equation (2):

$$\beta = \frac{\ln 10}{b} = \frac{2.303}{b} \qquad (3)$$

The inhibition efficiency was evaluated from the measured i_{corr} values using the following relationship:

$$\eta_{PP} = \frac{i^{0}_{corr} - i_{corr}}{i^{0}_{corr}} \times 100 \qquad (4)$$

where i^{0}_{corr} and i_{corr} are the corrosion current densities for mild steel electrode in the uninhibited and inhibited solutions, respectively.

The obtained parameters are listed in Table 2. It is observed that the inhibition efficiency increases with the inhibitor concentration to reach a maximum 10^{-3} M. This may be due to the inhibitors adsorption on mild steel/acid interface which prevented acid medium from attacking the metal surface [**26**].

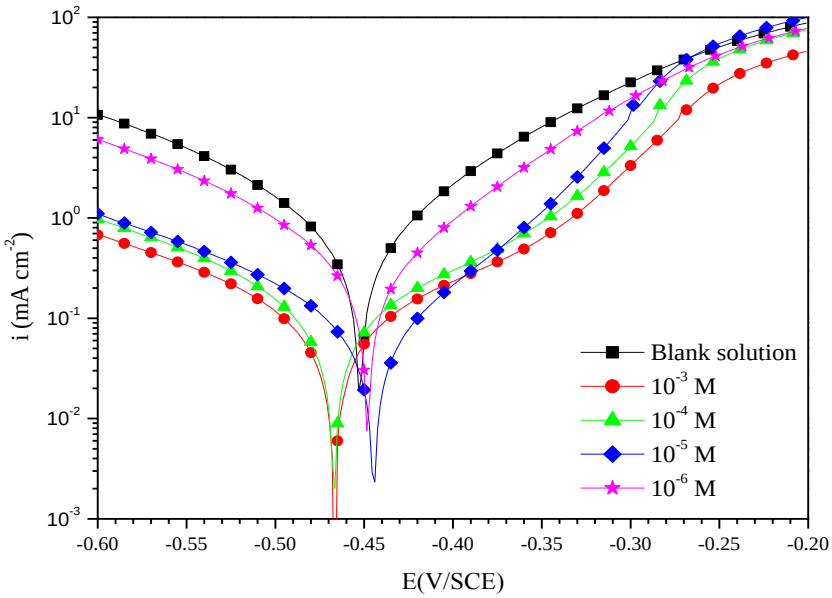

Figure 1 : Potentiodynamic polarization curves for mild steel in 1.0 M HCl containing different concentrations of **PTQ8** at 298 K.

Table 2. Electrochemical polarization parameters for mild steel corrosion in 1.0 M HCl with different concentrations of **PTQ8** at 298 K.

C_{inh} (M)	E_{corr} (mV/SCE)	$-\beta_c$ (mV dec^{-1})	i_{corr} (µA cm^{-2})	η_{PP} (%)
Blank solution	-454.4	101.1	590	-
10^{-6}	-451.9	79.9	220	62.1
10^{-5}	-471.5	127.1	81	86.05
10^{-4}	-471	104.5	71	87.7
10^{-3}	-449.3	108.1	48	91.8

3.3. Electrochemical impedance spectroscopy

The Nyquist and Bode representations at the open circuit potential for mild steel in the absence and presence of different concentrations of **PTQ8** are presented in Figures 2 and 3. The electrochemical parameters extracted from these diagrams using the proposed electrical circuit presented in Figure 4, are listed in Table 3.

The inhibition efficiencies were calculated using the following equation :

$$\eta_{EIS} = \frac{R^{inh}_{ct} - R_{ct}}{R^{inh}_{ct}} \times 100 \qquad (5)$$

R_{ct} and R_{ct}^{inh} are the charge-transfer resistance values in the absence and presence of inhibitor, respectively.

It is seen that the obtained diagrams were composed by one capacitive loop where its diameter increases with inhibitor addition due to the formation of a protective film on the mild steel surface. Generally, this type of diagram indicates that the corrosion reaction was controlled by transfer charges process on a heterogeneous and irregular surface electrode [**27,28**].

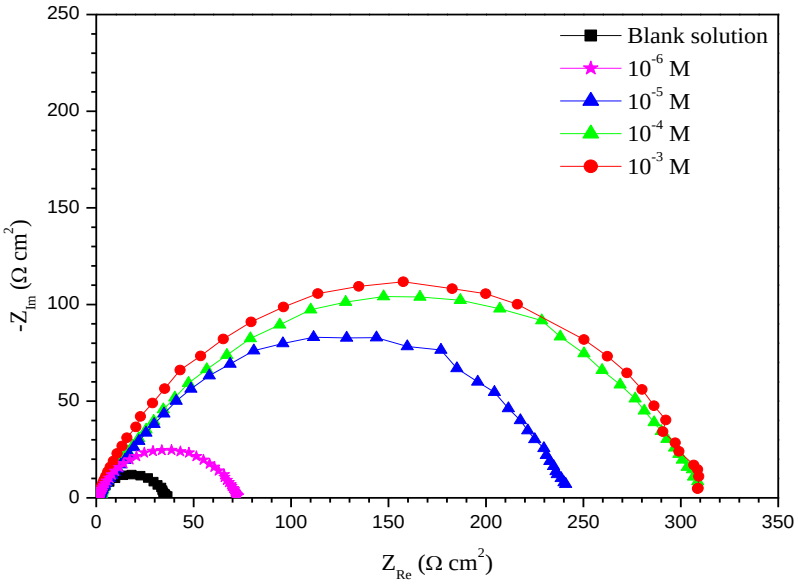

Figure 2: Nyquist plots of mild steel in 1.0 M HCl containing various concentrations of inhibitor at 298K.

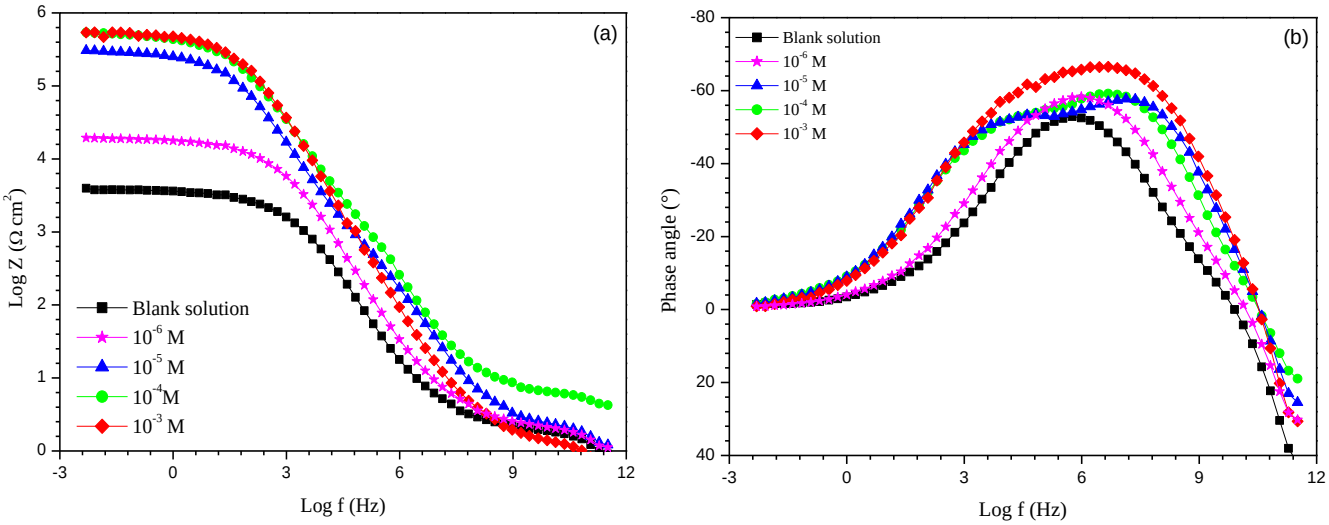

Figure 3. Bode plots (a) Module and (b) phase angle for mild steel in 1.0 M HCl in the absence and presence of different concentrations of **PTQ8**.

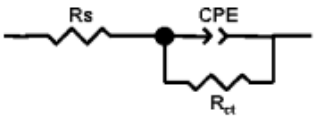

Figure 4: Equivalent electrical circuit corresponding to the corrosion process on the mild steel in hydrochloric acid.

Table 3: Electrochemical data for mild steel in 1.0 M HCl in the absence and presence of different concentrations of **PTQ8** at 298 K

C_{inh} (M)	R_{ct} (Ω cm^2)	C_{dl} (µF /cm^2)	η_{EIS} (%)
Blank solution	34.85	114.1	-
10^{-6}	71.37	89.19	51.1
10^{-5}	240.9	83.22	85.5
10^{-4}	308.1	51.64	88.6
10^{-3}	308.6	64.97	88.7

Examination of this table shows that the inhibitor addition decreases the double layer capacitance C_{dl} values and increases the charge transfer resistance R_{ct}. The inhibition efficiency values (η_{EIS} %) increases with the inhibitor

concentrations to reach a maximum of 88.7 % at 10^{-3} M. This indicated that the studied inhibitor forms a protective film on the mild steel surface. Also, the decrease in C_{dl} values suggesting that the protective film thickness increases with inhibitor concentrations.. These results confirm once again that the studied compound exhibit efficient inhibitive performance for mild steel in hydrochloric acid solution [**29**].

3.4. Effect of solution temperature

The influence of temperature on the inhibition efficiency of **PTQ8** in the temperature range from 298 K to 328 K, was also studied by potentiodynamic polarization curves and presented in Figure 5. The corrosion current densities (i_{corr}), the corrosion potential (E_{corr}), and the inhibitory efficiency are given in Table 3.

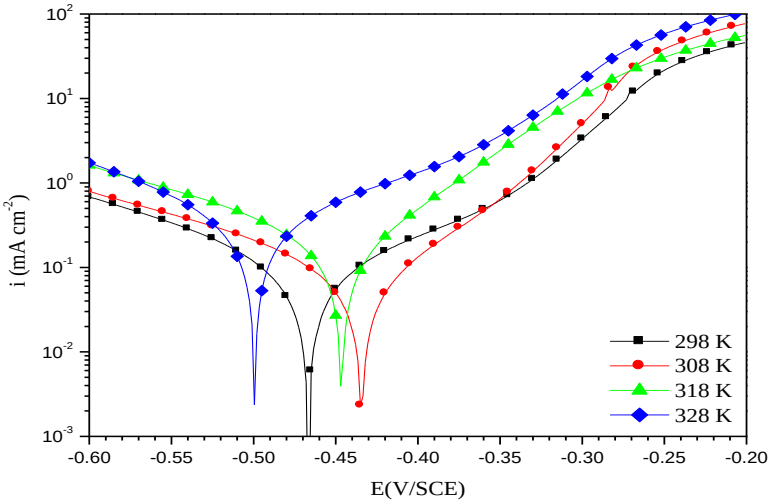

Figure 5: Potentiodynamic polarization curves for mild steel in 1.0M HCl in the presence of 10^{-3} M of **PTQ8** at different temperatures.

Table 4: Electrochemical parameters of mild steel in 1.0 M HCl without and with 10^{-3} M of **PTQ8** at different temperatures.

	T (K)	E_{corr} (mV/SCE)	$-\beta_c$ (mV dec^{-1})	i_{corr} (µA cm^{-2})	η_{PP} (%)
Blank solution	298	-454.4	101.1	0.590	-
	308	-451.1	104.9	0.820	-
	318	-454.8	111.1	1.324	-
	328	-464.3	101	2.368	-
10^{-3} M of **PTQ8**	298	-470.1	108.1	0.063	89.1
	308	-438.9	162	0.095	88.4
	318	-450.6	100.6	0.160	87.9
	328	-503.3	132.2	0.306	87

The results obtained from Table 3, reveal that the corrosion potential (E_{corr}) was modified by the increase of temperature from 298 K to 328 K without and with inhibitor. Indeed, the decrease in the inhibition efficiency with temperature was explained by the desorption of the inhibitor molecules from the metal surface at higher temperatures [**30,31**]. The activation parameters of the corrosion process were calculated at the different temperatures, without and with inhibitor addition. In addition, the activation energy (E_a) was determined using the i_{corr} values obtained from the potentiodynamic polarization curves, according to equation [**32**] :

$$i_{corr} = K \exp(-\frac{E_a}{RT}) \qquad (6)$$

where i_{corr} is the corrosion current density, E_a is the activation energy for the corrosion process, *K* is the Arrhenius pre-exponential constant, T is the absolute temperature and R is the universal gas constant.

Figure 6 illustrates the variation of the corrosion current density logarithm as a function of the absolute temperature inverse. It is obtained that this variation of Ln i_{corr} = f (1/T) was a straight line for both cases in the absence and presence of **PTQ8**.

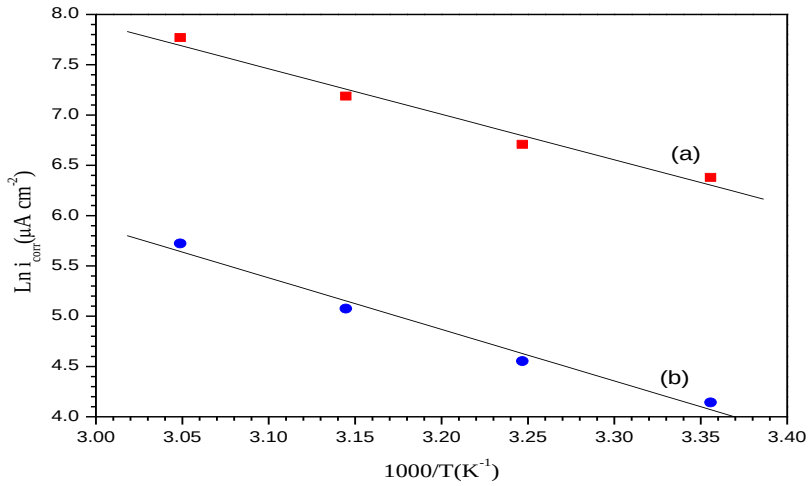

Figure 6: Arrhenius plots of mild steel in 1.0 M HCl (a) without and (b) with 10^{-3} M of **PTQ8**

An alternative formula of the Arrhenius equation which can determine the activation enthalpy (ΔH^*_a) and entropy (ΔS^*_a) using the following equation:

$$i_{corr} = \frac{RT}{Nh}\exp\left(\frac{\Delta S^*_a}{R}\right)\exp\left(\frac{\Delta H^*_a}{RT}\right) \quad (5)$$

where i_{corr} is the corrosion current density, h is the Planck's constant, N is the Avogadro number and R is the universal gas constant.

The activation enthalpy and entropy values for mild steel corrosion in 1.0 M HCl in the absence and presence of 10^{-3} M of **PTQ8** can be evaluated from the slope and intercept of the curve of Ln (i_{corr}/T) versus 1/T, respectively as shown in Figure 7.

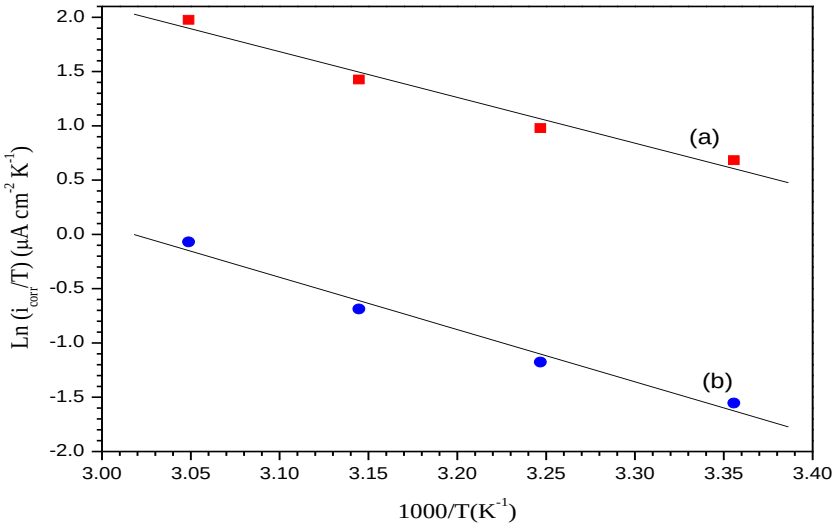

Figure 7: Relation between Ln (i_{corr}/ T) and 1000/T at different temperatures

In 1.0 M HCl solution, the addition of **PTQ8** leads to an increase in the apparent activation energy E_a from 37.64 kJ mol^{-1} to 42.64 kJ mol^{-1}. This result show that the addition of **PTQ8** decreases metal dissolution in 1.0 M HCl medium and that it is to the phenomenon of physisorption [**33,34**]. The positive sign of ΔH^*_a which is increases from 35.04 kJ mol^{-1} to 40.04 kJ mol^{-1}, reflects the endothermic nature of the mild steel dissolution process indicating that the metal dissolution is slow in the presence of inhibitor [**35**]. The large negative value of ΔS^*_a which is slightly increases negatively from -75.03 J mol^{-1} K^{-1} to - 76.82 J mol^{-1} $K^{-}1$, implies that there is decrease of the disorder during the transformation of the reactants into complex. [**36**]

3.5. Adsorption isotherm

The adsorption isotherms are then an important complement able of determining the electrochemical mechanism which leads to the adsorption of this organic compound on the metal surface. The adsorption of **PTQ8** at 298 K on the mild steel surface in 1.0 M HCl solution obeys the Langmuir adsorption isotherm [**37**]:

$$\frac{C_{inh}}{\theta} = \frac{1}{K_{ads}} + C_{inh} \qquad (7)$$

where C_{inh} is the inhibitor concentration, θ is the surface coverage and K_{ads} is the adsorption equilibrium constant. The Langmuir approach is based on a molecular kinetic model of the adsorption– desorption process. On the other hand, the adsorption equilibrium constant (K_{ads}) is related to the free energy of adsorption (ΔG^*_{ads}) of the inhibitor by applying the equation [**38**]:

$$K_{ads} = \frac{1}{55.55} \exp\left(-\frac{\Delta G^*_{ads}}{RT}\right) \qquad (8)$$

where R is the universal gas constant, T is the absolute temperature and 55.55 represent the molar concentration of water in the solution.

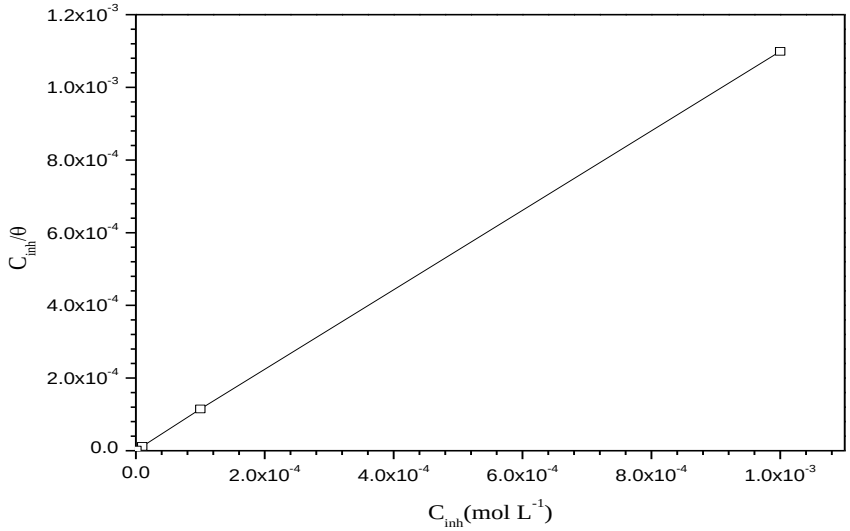

Figure 8 : Langmuir adsorption isotherm of **PTQ8** on mild steel surface in 1.0 M HCl at 298 K

Generally, the ΔG^*_{ads} values close to -20 kJ mol^{-1} corresponded to the electrostatic interactions between the charged molecules and the metal charges (physisorption). On the other hand, when the ΔG^*_{ads} is close to -40 kJ mol^{-1} a transfer of charges between the inhibitor molecules and metal surface by forming covalent bonds was established (chemisorption) [**39,40**]. In this study, the ΔG^*_{ads} value is close to -42.4 kJ mol^{-1} which is large negative indicated that the adsorption of the inhibitor molecules on mild steel surface was spontaneous and the coordinate covalent bond was formed by the charge sharing or transferring from the inhibitor molecules to the metal surface [**41,42**].

3.6. Quantum chemical calculation

3.6.1. DFT calculations

In order to understand the inhibition mechanism of mild steel corrosion by **PTQ8** at the molecular level, quantum chemical computations was carried out. The optimized structures, HOMO (highest occupied molecular orbital), and LUMO (lowest unoccupied molecular orbital) are represented in Figure 9.

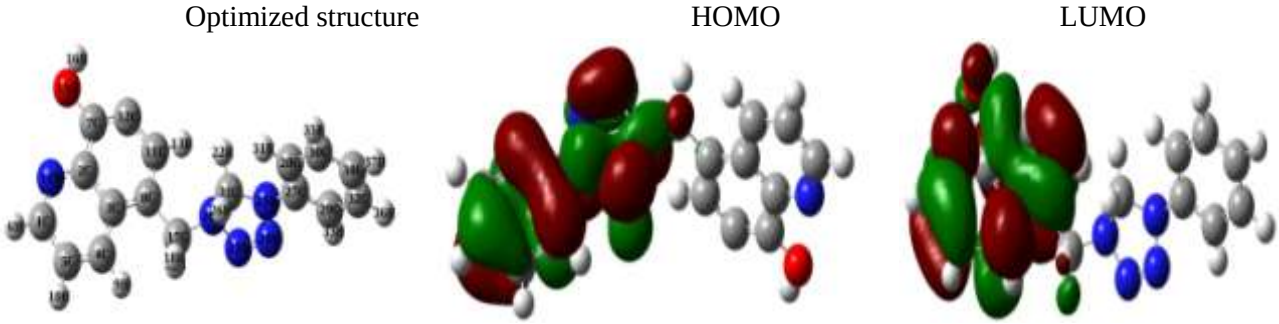

Figure 9: Quantum chemical results, calculated at DFT/B3LYB/6-31G (d, p).

Charge distribution and direction of dipole moment (μ)**,** the contour and the surface representation of the electrostatic potential of **PTQ8** are also presented in Figures 10 and 11. In this regard, important reactivity

parameters such as the energy of the highest occupied molecular orbital (E_{HOMO}), that of the lowest unoccupied molecular orbital's (E_{LUMO}), the energy gap (ΔE), and molecular dipole moment were calculated and given in Table 5. Figure 9 showed that the electron density distribution of HOMO was localized on the molecular surface of phenyltetrazolidinyl of **PTQ8**. On the other hand, the electronic density LUMO is distributed on the molecule surface of quinoline **PTQ8**.Figure 10 showed that the **PTQ8** has a remarkable excess of negative charge around nitrogen, oxygen and some carbon atoms, indicating that these are the coordinating sites of the tested inhibitor.

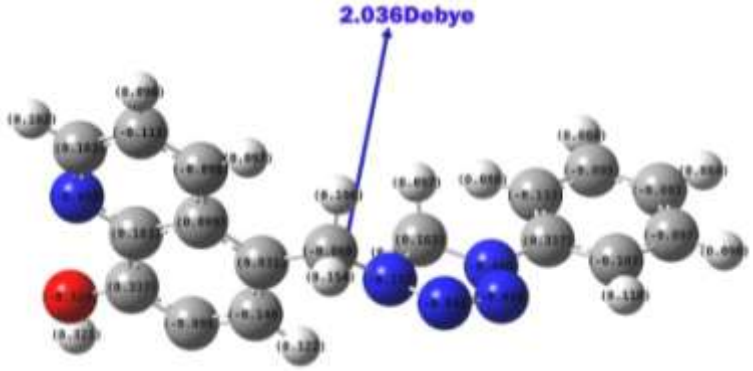

Figure 10: Charge distribution and direction of dipole moment (μ) of **PTQ8**.

The electrostatic potential is considered predictive of chemical reactivity because the negative potential regions are expected to be sites of protonation and nucleophilic attack, while the positive potential regions may indicate electrophilic sites. Figure 11 shows the molecular electrostatic potential (MEP) and the electrostatic potential of the potential Maps. It can be seen that the electrostatic potential around some groups of C-H is positive (blue color) while the electrostatic potential regions around the nitrogen and oxygen atoms are negative (red color).

Contour electrostatic potential | Electrostatic potential maps

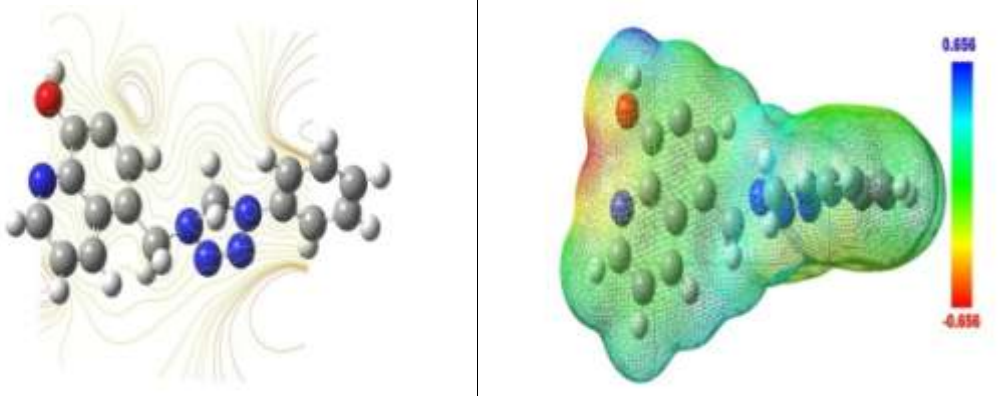

Figure 11: Contour electrostatic potential and electrostatic potential maps around the molecule of **PTQ8**.

It is observed also that the molecule has a large E_{HOMO} will act as an electron donor to an appropriate acceptor which has a low E_{LUMO} where the molecular orbitals are empty. The high values of E_{HOMO} thus facilitate the adsorption of the inhibitor molecules on the metallic surface and therefore the inhibition efficiency by influencing the electron transfer process through the adsorbed layer [**22**,**43**]. The difference $\Delta E = E_{LUMO} - E_{HOMO}$ (gap energy) is the minimum energy required to excite an electron in a molecule. When ΔE decreases, the reactivity of the inhibitor to the iron surface increases [**44,45**]. According to Table 5, the high value of E_{HOMO}, lower value of E_{LUMO} and a small ΔE indicates a higher interaction between the metal surface and inhibitor molecules [**46,47**]. However, the higher dipole moment (μ) value of **PTQ8** suggested that it has a stronger dipole-dipole interaction with mild steel [**48**]. In addition, the electron transfer number (ΔN) was calculated using the following equation [**48**]:

$$\Delta N = \frac{\chi_{Fe} - \chi_{inh}}{2\left(\eta_{Fe} + \eta_{inh}\right)} \qquad (9)$$

where χ_{Fe} and χ_{inh} denote the absolute electronegativity of iron and the inhibitor molecule, respectively, and η_{Fe} and η_{inh} denote the absolute hardness of iron and the inhibitor molecule, respectively. The χ_{Fe} and η_{Fe} values are taken as 7 eV mol^{-1} and 0 eV mol^{-1}, respectively [**49,50**]. If $\Delta N < 3.6$, the inhibition efficiency increases with the increase in electron-donation ability from the inhibitor to the metallic surface [**22**]. The results, as reported

in Table 5, show the high electron transfers number, which also confirms that **PTQ8** has the highest inhibition performance. This finding suggested that the inhibition efficiency increases with increasing softness and decreases with increasing the hardness of the inhibitor molecules. Absolute electronegativity (χ), global hardness (η) and global softness (σ) are estimated using the equations [**51,52**]:

$$\chi = \frac{I + A}{2} \quad (10)$$

$$\eta = \frac{I - A}{2} \quad (11)$$

$$\sigma = \frac{1}{\eta} = -\frac{2}{E_{HOMO} - E_{LUMO}} \quad (12)$$

The ionization potential (I) and the electron affinity (A) are defined as follows equations :

$I = -E_{HOMO}$ (13)

$A = -E_{LUMO}$ (14)

Table 5: Quantum theoretical parameters for **PTQ8** calculated using B3LYP/6-31G (d,p)

Parameters	E_{LUMO} (eV)	E_{HOMO} (eV)	ΔE (eV)	μ (debyes)	η (eV)	σ (e V^{-1})	I (eV)	χ (eV)	A (eV)	ΔN (eV)	TE (u a)
PTQ8	-5.552	-1.523	4.029	2.036	2.014	0.496	1.523	3.537	5.552	0.859	-1005.077

3.6.2. Fukui functions (Fig. 6)

One of the most important factors to determine the applications of molecular system is its reactivity. For experimental and theoretical chemist identify the reactive sites is very important, the Fukui function provides us with a measure of the change in the density with respect to a change in the number of electrons [**49,53,54**].

Table 6: Fukui function values considering NPA of **PTQ8** molecule calculated at the B3LYP / 6-31 G (d, p).

Atomes	P(N)	P (N+1)	P (N-1)	f_k^+	f_k^-
C1	5.966	5.939	6.006	-0.027	-0.040
C2	5.850	5.837	5.869	-0.013	-0.019
C3	6.083	6.078	6.100	-0.005	-0.017
C4	6.188	6.178	6.206	-0.010	-0.018
C5	6.276	6.246	6.325	-0.030	-0.049
C7	5.758	5.733	5.742	-0.025	0.016
C8	6.050	6.024	6.108	-0.026	-0.058
C11	6.312	6.311	6.254	-0.001	0.058
C12	5.925	5.808	6.435	-0.117	-0.510
N14	7.423	7.381	7.442	-0.042	-0.019
O15	8.664	8.624	8.716	-0.04	-0.052
C17	6.274	6.284	6.268	0.010	0.006
N20	7.331	7.276	7.302	-0.055	0.029
C21	6.096	6.114	6.094	0.018	0.002
N22	7.034	6.989	7.028	-0.045	0.006
N23	7.033	6.991	7.075	-0.042	-0.042
N24	7.284	7.215	7.288	-0.069	-0.004
C27	5.844	5.842	5.832	-0.002	0.012
C28	6.284	6.254	6.285	-0.030	-0.001
C29	6.259	6.223	6.265	-0.036	-0.006
C30	6.220	6.209	6.224	-0.011	-0.004
C32	6.219	6.211	6.227	-0.008	-0.008
C34	6.261	6.189	6.279	-0.072	-0.018

The Fukui functions can be defined using finite differences of the electronic density [**55,56**].

$f_k^+ = P_k(N+1) - P_k(N)$ (For nucleophilic attack) (15)

$f_k^- = P_k(N) - P_k(N-1)$ (For electrophilic attack) (16)

where, P_k (N), P_k(N+1) and P_k(N-1) are the natural populations for the atom k in the neutral, anionic and cationic species, respectively.

The interpretation of numerical values of the Fukui function is as follows: The active site for nucleophilic attacks is the atom in the molecule where f_k^+ has the highest value while the site for electrophilic attack is the atom in the molecule where the value f_k^- is the highest [**53,57**].

It can be seen that the preferred sites for electrophilic attack are the C7, C11, C20 and C27. On the other hand, C17 and C21 are the susceptible sites for nucleophilic attacks as they present the highest values of f_k^+. The information obtained from the Fukui condensed function entirely agrees with the analysis of the Natural Population analysis (NPA) and Frontier molecular orbitals.

Conclusion

PTQ8 inhibits mild steel corrosion in 1.0 M HCl solution. Its inhibition efficiency increases with concentrations while decreases with temperature. It is found that the charge transfer resistance increases and double layer capacitance decreases with **PTQ8** addition due to the adsorption of the inhibitor molecules on the mild steel surface. The adsorption of the tested inhibitor follows Langmuir adsorption isotherm. Quantum chemical calculation by DFT method was performed to identify the reactivity of tested molecules towards corrosion inhibition, and the results are in good agreement with the experimental investigations.

References

1. I. Dehri, M. Özcan, *Mat. Chem. Phy.* 98 (2006) 316.
2. A. El ouafi, B. Hammouti, H. Oudda, S. Kertitb, M. Benkaddour, T. Ben-hadda, *In annales de chimie science des matériaux*. 27 (2002) 71.
3. M. Belayachi, H. Serrar, A. El Assyry, H. Oudda, S. Boukhris, M. Ebn Touhami, A. Zarrouk, B. Hammouti, Eno E. Ebenso, A. El Midaoui, *Int. J. Electrochem. Sci*. 10 (2015) 3038.
4. A. Ghazoui, R. Saddik, N. Benchat, B. Hammouti, M. Guenbour, A. Zarrouk, M. Ramdani, *Der Pharm. Chem*. 4 (2012) 352.
5. H. Zarrok, R. Saddik, H. Oudda, B. Hammouti, A. El Midaoui, A. Zarrouk, N. Benchat, M. Ebn Touhami, *Der Pharm. Chem*. 3 (2011) 272.
6. A. Zarrouk, B. Hammouti, R. Touzani, S.S. Al-Deyab, M. Zertoubi, A. Dafali, S. Elkadiri, *Int. J. Electrochem. Sci*. 6 (2011) 4939.
7. A. Zarrouk, B. Hammouti, A. Dafali, H. Zarrok, *Der Pharm. Chem*. 3 (2011) 266.
8. A. Ghazoui, A. Zarrouk, N. Bencaht, R. Salghi, M. Assouag, M. El Hezzat, A. Guenbour, B. Hammouti, *J. Chem. Pharm. Res*. 6 (2014) 704.
9. H. Zarrok, A. Zarrouk, R. Salghi, H. Oudda, B. Hammouti, M. Assouag, M. Taleb, M. Ebn Touhami, M. Bouachrine, S. Boukhris, *J. Chem. Pharm. Res*. 4 (2012) 5056.
10. H. Zarrok, A. Zarrouk, R. Salghi, M. Assouag, B. Hammouti, H. Oudda, S. Boukhris, S.S. Al Deyab, I. Warad, *Der Pharm. Lett*. 5 (2013) 43
11. M. Belayachi, H. Serrar, H. Zarrok, A. El Assyry, A. Zarrouk, H. Oudda, S. Boukhris, B. Hammouti, E.E. Ebenso, A. Geunbour, *Int. J. Electrochem. Sci*. 10 (2015) 3010.
12. A. Zarrouk, H. Zarrok, R. Salghi, R. Touir, B. Hammouti, N. Benchat, L.L. Afrine, H. Hannache, M. El Hezzat, M. Bouachrine, *J. Chem. Pharm. Res*. 5 (2013) 1482.
13. H. Zarrok, A. Zarrouk, R. Salghi, M. Ebn Touhami, H. Oudda, B. Hammouti, R. Touir, F. Bentiss, S.S. Al-Deyab, *Int. J. Electrochem. Sci*. 8 (2013) 6014.
14. D. Ben Hmamou, M.R. Aouad, R. Salghi, A. Zarrouk, M. Assouag, O. Benali, M. Messali, H. Zarrok, B. Hammouti, *J. Chem. Pharm. Res*. 4 (2012) 34984.
15. S.A. Abd El-Maksoud, *Appl. Surf. Sci.* 206 (2003) 129.
16. S. Kertit, B. Hammouti, *Appl. Surf. Sci.* 161 (1996) 59.
17. H.H. Hassan, E. Abdelghani, M.A. Amina, *Electrochim. Acta.* 52 (2007) 6359.
18. A.A. Watson, G.W.J. Fleet, N. Asano, R.J. Molyneux, R.J. Nugh, *Phytochemistry.* 56 (2001) 265.
19. G.J. Atwell, B.C. Baguley, W.A. Denny, *J. Med. Chem.* 32 (1989) 396.
20. M. El Faydy, M. Galai, R. Touir, A. El Assyry, M. Ebn Touhami, B. Benali, B. Lakhrissi, A. Zarrouk, *J. Mater. Environ. Sci.* 7 (4) (2016) 1406-.

21. S. Lahmidi, A. Elyoussfi, A. Dafali, H. Elmsellem, N.K. Sebbar, L. El Ouasif, A.E. Jilalat, B. El Mahi, E.M. Essassi, I. Abdel-Rahman, B. Hammouti, *J. Mater. Environ. Sci.* 8 (2017) 225.
22. I. Lukovits, E. Kalman, F. Zucchi, *Corrosion.* 57 (2001) 3.
23. M. J. Frisch, G. W. Trucks, H. B. Schlegel, and al., Gaussian 03, Revision C.02.
24. A. Anejjar, R. Salghi, A. Zarrouk, O. Benali, H. Zarrok, B. Hammouti, E.E. Ebenso, *J. Assoc. Arab Univ. Basic Appl. Sci.* 15 (2014) 21.
25. M. Mobin, M. Rizvi, *Carbohydr. Polym.* 136 (2016) 384.
26. A. Ghazoui, N. Bencaht, S.S. Al-Deyab, A. Zarrouk, B. Hammouti, M. Ramdani, M. Guenbour, *Int J Electrochem Sci.* 8 (2013) 2272.
27. M. Moradi, J. Duan, X. Du, *Corros. Sci.* 69 (2013) 338.
28. E. Cafferty, N. Hackerman, *J. Electrochem. Soc*. 119 (1972) 146.
29. M. Elfaydy, H. Lgaz, R. Salghi, M. Larouj, S. Jodeh, M. Rbaa, H. Oudda, K. Toumiat, B. Lakhrissi, *J. Mater. Environ. Sci.* 7 (9) (2016) 3193.
30. M. Mihit, S. El Issami, M. Bouklah, L. Bazzi, B. Hammouti, E. Ait Addi, R. Salghi, S. Kertit, *Appl. Surf. Sci.* 252 (2006) 2389.
31. M. Mihit, K. Laarej, H. Abou El Makarim, L. Bazzi, R. Salghi, B. Hammouti, *Arab. J. Chem.* 3 (2010) 5.
32. R. Villamil, P. Corio, J. Rubim, S. Agostinho, *J. Electroanal. Chem.* 535 (2002) 75.
33. R. Liu, Y. Qiao, M. Yan, Y. Fu, *J. Mater. Sci. Technol.* 28 (2012) 1046.
34. W. Durnie, R. Marco, A. Jefferson, B. Kinsella, *J. Electrochem. Soc.* 146 (1999) 1751.
35. N.M. Guan, L. Xueming, L. Fei, *Mater. Chem. Phys.* 86 (2004) 59.
36. S.M.A. Hosseini, M. Salari, M. Ghasemi, M. Abaszadeh, *Z. Phys. Chem.* 223 (2009) 769.
37. I.B. Obot, A. Madhankumar, *J. Ind. Eng. Chem.* 25 (2015) 105.
38. N.O. Eddy, H. Momoh-Yahaya, E.E. Oguzie, *J. Adv. Res.* 6 (2) (2015) 203.
39. S. Deng, X. Li, H. Fu, *Corros. Sci.* 53 (2011) 822.
40. S. Safak, B. Duran, A. Yurt, G. Türkoğlu, *Corros. Sci.* 54 (2012) 251.
41. A. Ehsani, M. Nasrollahzadeh, M.G. Mahjani, R. Moshrefi, H. Mostaanzadeh, *Ind J., Eng. Chem.* 20 (6) (2014) 4363.
42. A. Biswas, S. Pal, G. Udayabhanu, *Appl. Surf. Sci.* 353 (2015) 173.
43. N. Khalil, *Electrochim. Acta.* 48 (2003) 2635.
44. D. Zhang, L. Gao, G. Zhou, *Corros. Sci.* 46 (2004) 3031.
45. Y. Feng, S. Chen, Q. Guo, Y. Zhang, *J. Electroanal. Chem.* 602 (2007) 115.
46. K. Ramya, R. Mohan, K.K. Anupama, A. Joseph, *Mater. Chem. Phys.* 149 (2015) 632.
47. I. Danaee, O. Ghasemi, G.R. Rashed, M. Rashvand Avei, M.H. Maddahy, *J. Mol. Struct.* 1035 (2013) 247.
48. K. Ismaily Alaoui, F. El Hajjaji, M. Azaroual, M. Taleb, A. Chetouani, B. Hammouti, F. Abrigach, M. Khoutoul, Y. Abboud, A. Aouniti, R. Touzani, *J. Chem. Pharm. Res.*, 6(7) (2014) 63-81
49. Z. El Adnani, M. Mcharfi, M. Sfaira, M. Benzakour, A. Benjelloun, M. Ebn Touhami, *Corros. Sci.* 68 (2013) 223.
50. K. Zhang, B. Xu, W. Yang, X. Yin, Y. Liu, Y. Chen, *Corros. Sci.* 90 (2015) 284.
51. N.O. Eddy, H. Momoh-Yahaya, E.E. Oguzie, *J. Adv. Res.* 6 (2015) 203.
52. L.O. Olasunkanmi, M.M. Kabanda, E.E. Ebenso, *Phys. E Low-Dimens. Syst. Nanostructures.* 76 (2016) 109.
53. L. Feng, H. Yang, F. Wang, *Electrochimica Acta.* 58 (2011) 427.
54. H. Jafari, K. Sayin, *J. Taiwan Inst. Chem. Eng.* 56 (2015) 181.
55. J. Saranya, P. Sounthari, K. Parameswari, S. Chitra, *Measurement.* 77 (2016) 175.
56. S. Kaya, B. Tüzün, C. Kaya, I.B. Obot, *J. Taiwan, Inst. Chem. Eng.* 58 (2016) 528.
57. S. RameshKumar, I. Danaee, M. RashvandAvei, M. Vijayan, *J. Mol. Liq.* 212 (2015) 168.

(2018) ; http://www.jmaterenvironsci.com